Simulations of the BOLD effect using a realistic model of the vasculature

J. P. Marques[1], R. W. Bowtell[1]

[1]Sir Peter Mansfield Magnetic Resonance Centre,School of Physics and Astronomy, University of Nottingham, Nottingham, Nottinghamshire, United Kingdom

INTRODUCTION Although functional magnetic resonance imaging based on blood oxygenation level dependent (BOLD) contrast has become a widely used tool in neuroscience, the physiological changes that underpin the BOLD effect are still not completely understood. In particular the relationship between the changes in blood oxygenation, occurring in active brain tissue, and the variation in signal intensity in T_2^*-, or T_2-weighted images is not well characterised. In probing this relationship, it has generally been assumed that the brain vasculature can be represented as an arrangement of randomly oriented, infinite cylinders of varying size (1, 2). Here, we probe the effect of this assumption by using a 3D finite element method to simulate BOLD signal changes produced by infinite cylinders and a more realistic model of the human cortical vasculature, based upon scanning electron microscopy measurements of the terminal vascular bed in the superficial cortex of the rat (3).

METHODS The models were compared by simulating the evolution of magnetisation in two different environments of magnetic field inhomogeneity:

(i) the Infinite Cylinders Model (ICM), for which analytical forms of the field variation are well known. The results of simulations employing different vessel orientations were integrated in order to yield the signal of a voxel containing vessels with an isotropic distribution of orientations;

(ii) the Realistic Vasculature Model (RVM) used as a starting point a distribution of magnetic susceptibility, χ, given by the rat brain microcirculation model, as shown in Fig. 1. The field shift maps, an example of which is shown in Fig. 2, were calculated using a FFT method, in which field shift, B_{dz}, and susceptibility are directly related in k-space by $B_{dz}(\mathbf{k}) = B_0\left(\cos^2(\beta) - 1/3\right)\chi(\mathbf{k})$. Here B_0 is the applied static magnetic field and β is the angle between the direction of the main magnetic field and **k** (4).

The evolution of the magnetization during a gradient echo (GE) or spin echo (SE) sequence was calculated by numerically applying the Bloch Equations, taking into account the effects of relaxation, frequency shifts due to field inhomogeneities and diffusion. At each time step, the integrated effects (as opposed to the incremental effects which yield a more stringent convergence criterion) of field inhomogeneity and relaxation on the transverse magnetization were applied using the Bloch equation $M^+(\mathbf{r}, t+\delta t) = (M^+(\mathbf{r},t)e^{i\gamma B_{dz}(\mathbf{r})\delta t} + D(\mathbf{r})\nabla^2 M^+(\mathbf{r},t))e^{-\delta t/T_2}$.

Only the term reflecting the effect of diffusion has to be calculated at each time step, while the others may be calculated only once at the star of the simulation. The diffusion term was calculated using a finite difference solution, imposing restrictions at the grey matter/vessel boundaries where reflection was considered to occur. The maximum allowed time step, δt, is set by the largest diffusion coefficient, D, and the distance between neighbouring pixels (δx, δy, δz), via $\delta t=(\delta x^2+\delta y^2+\delta z^2)/(6D)$ or by the desired temporal resolution.

Calculations were carried out using blood/tissue susceptibility difference ($\Delta\chi$) values of 0.45 ppm (oxygenation fraction, Y=0.5), 0.36 ppm (resting state Y=0.6), 0.27ppm (intermediate state Y=0.7) and 0.18 ppm (activated state Y=0.8), and a blood volume fraction of 1.25%, 2.5%, 3.75% and 4% (the value set by the form of the RVM was of 1.25%). Diffusion coefficients of $1.45\text{x}10^{-9}\text{m}^2\text{s}^{-1}$ inside and $0.7\text{x}10^{-9}\ \text{m}^2\text{s}^{-1}$ outside vessels were employed. For the SE simulation the echo time was set to the T_2 of grey matter (the values used for relaxation time were those at 3T). Several length scales were considered (by simply rescaling the distance between neighbouring pixels), so that a wide range of vessel diameters from capillaries (4μm) to large venules (300μm) was simulated. Finally to calculate the dependences of R_2 and R_2^* on the total blood fraction and χ, the differences of these quantities from the initial R_2 of GM were summed over calculations made at different length scales. The validity of this approach is based on the observation that the number of vessels N(d) with a specific diameter, d, scales as $1/d^3$ (5), while the volume corresponding to the RVM scales with d^3. By making such a sum, the small vessels are considered as having an additive background effect on the relaxation rate due to larger vessels.

Two different matrix sizes (32^3 and 64^3) were used in the ICM to test whether reduction of pixel resolution would be an issue when simulating the RVM (128^3 is the largest matrix size that could be simulated in an acceptable time of 30 hours). Simulations of the ICM in a 32^3 matrix were also performed using a field map calculated via the FFT rather than the analytical method, to ensure that the FFT method did not introduce any intrinsic difference. No significant differences in the ICM contrast were observed when reducing the matrix size or calculating the field shift with the FFT method, leading us to believe that the differences in the results are not due to the methodology used, but to the model under study.

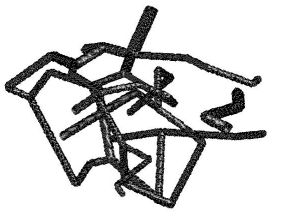

Fig. 1 Realistic Vascular Model based upon SEM of the rat cortex(3)

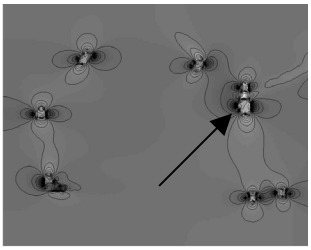

Fig. 2 Frequency shifts generated in one slice of the RVM

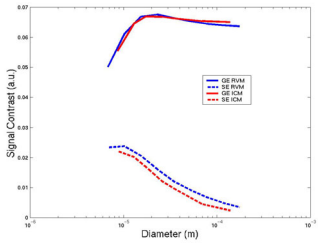

Fig. 3 Signal change between activated and resting state as a function of the average vessel diameter for a blood volume fraction of 3.75%

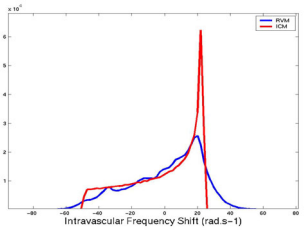

Fig. 4 Intravascular frequency shift at 3 Tesla

RESULTS Figure 3 shows the dependence of GE and SE contrast (signal difference between active and resting states) on the (average) diameter of the vessels both for the ICM and for the RVM. This shows a very good agreement between the ICM and RVM for the form of the dependence of the BOLD effect on vessel diameter. The main difference between the two models seems to be in the intravascular contribution to contrast. In Fig. 4 intravascular frequency distributions generated by the ICM and those found in the RVM, considering 5 different orientations of the model with respect to B_0, are shown. The difference can be partially explained by the fact that vessels in the RVM experience fields generated by neighbouring vessels. Such effects will be most relevant at junctions between vessels (the arrow in Fig. 2 indicates the location of such a junction). This effect leads to an increase of the intravascular contribution to the BOLD contrast (3% in the ICM to 11% in the RVM at the maximum BOLD contrast).

An interesting measure obtained was the value of the variability of BOLD contrast with the angle between the z-axis of the RVM and the direction of B_0 for a length scale comparable to the size of a pixel in an fMRI study. The variability was found to be of approximately 6%.

Finally we found the following dependence on B_0(T), V(%) and $\Delta\chi$ (ppm) for the relaxivity: $R_2=R_{2GM}(B_0)+0.1430(\pm0.008)B_0^2V\Delta\chi^2$ and $R_2^*= R_2^*{}_{GM}(B_0)+1.08(\pm0.03)B_0V\Delta\chi$. These variations are a consequence of the dependence of R_2 on diffusion in magnetic field gradients, and the dependence of R_2^* on static dephasing.

CONCLUSION AND FUTURE WORK Using a realistic model of the vasculature to simulate the BOLD effect brings a new insight into the importance of different contributions to the overall BOLD contrast. The effect of flow is now being evaluated. Preliminary studies indicate that flow causes a line narrowing of the intravascular signal that can be understood as a reduction of the phase accumulation experienced by each individual spin due to movement through the network of vessels in which there is a significant distribution of field shifts.

REFERENCES (1) Yablonsky *et al*, *Magn.Res.Med*, **32**, 749-763, 1994. (2) Boxerman *et al*, *Magn Reson Med*, **34**,555-566, 1995. (3) E. Motti *et al*., *J. Neurosurg*, **65**, 834-846, 1986. (4) Marques *et al*, Proc. Int. Soc. Mag. Reson. Med. 11 (2003) P-1020, (5) Turner R. Neuroimage **16**, 1062-1067 (2002).